Resolution effects on hydrodynamical simulations of stellar atmospheres

by Regner Trampedach

July 14, 1998

1 Introduction

I have studied the effects of varying the resolution of the hydrodynamical simulations of convection (using the hydrocode by Åke Nordlund and Robert F. Stein) by comparing the simulations listed in Tab. 1. In particular, this is an attempt to make a rigorous comparison in order to disentangle the effects of some of the many differences between the many simulations we now have at our disposal.

Table 1: Parameters for the simulations.

name	$T_{\rm eff}/[{\rm K}]$	$g_{\rm surf}$	N_x/N_z	$[\nabla_{\rm s}]$	$\left[\frac{P_{\rm turb}}{P_{\rm tot}}\right]$	$\left[\frac{P_{\rm turb}}{P_{\rm tot}}\right]^*$	comp.
sol32	5640 ± 35	27500.0	32/41	0.46	7.26%	8.16%	Gus.
sol63	5677 ± 25	27500.0	63/63	0.57	10.86%	11.52%	Gus.
sol125	5774 ± 9	27500.0	125/82	0.66	12.52%	12.56%	Gus.
sol50G	5802 ± 14	27395.9	50/82	0.73	10.73%	10.56%	Gus.
sol50	5797 ± 6	27395.9	50/82	0.66	11.10%	10.97%	AG89
sol100	5777 ± 8	27395.9	100/82	0.68	12.59%	12.59%	AG89
Pro50z	6513 ± 18	10840.0	50/82	0.70	22.28%	22.04%	Gus.
Pro50	6470 ± 15	10840.0	50/82	0.73	21.03%	21.03%	Gus.

The brackets [...] denote the maximum of the content, interpolated to a very fine grid, in order to resolve even very sharp peaks on a coarse grid. Column 7 of Tab. 1 is the maximum of the pressure ratio from column 6, corrected for the differences in $T_{\rm eff}$ and $g_{\rm surf}$ according to the expression

$$\Delta\frac{P_{\rm turb}}{P_{\rm tot}} = 84.519941\Delta\log T_{\rm eff} - 9.994203\Delta\log g_{\rm surf}, \qquad (1)$$

found from fitting the pressure ratios from my 7 simulations with Gustafsson composition and $50 \times 50 \times 82$ resolution, to $a + b\log T_{\rm eff} + c\log g_{\rm surf}$. sol100 is used as the reference point for the solar simulations and Pro50 for the Procyon simulations.

2 The vertical resolution

In Fig. 1 I compare the z-scales of sol32, sol63 and sol125, together with sol100 which differs from the others in the chemical composition. The grid spacing Δz has been scaled to the number of z-points, N_z, in order to filter out the resolution effects and show the distribution effects instead (scaled to show the actual grid Δz for $N_z = 82$).

Notice the ragged Δz for the sol125, which apart from that follows the sol32 closely. The sol63 on the other hand, has comparatively lower resolution in the atmosphere but the "kink" lies deeper.

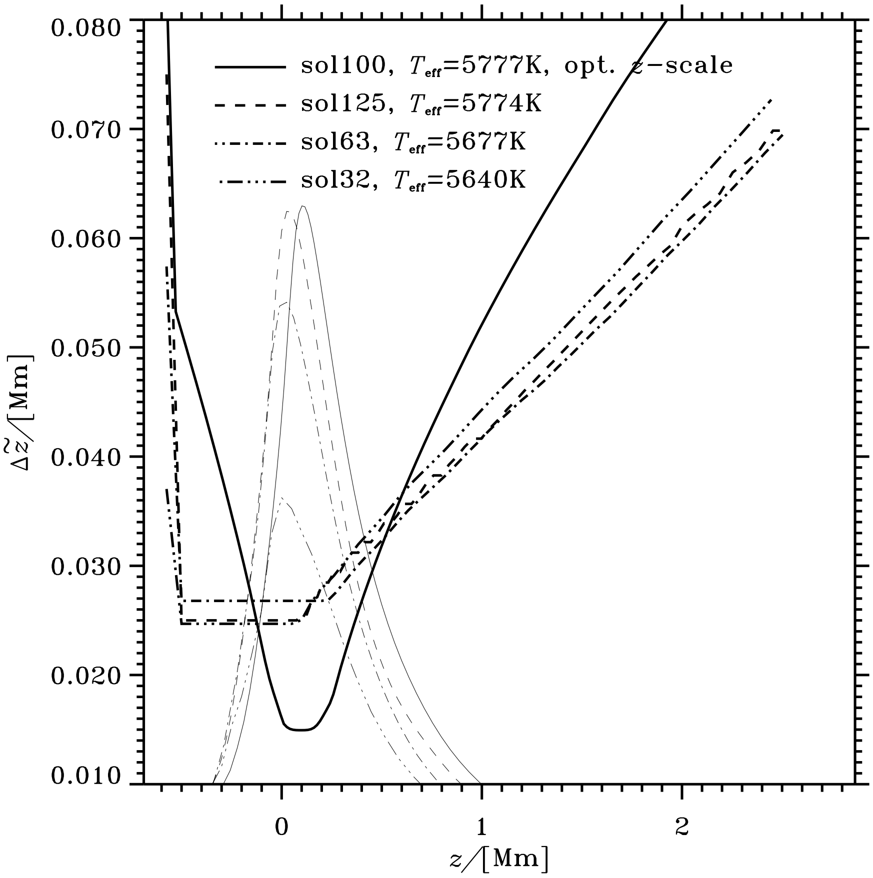

Figure 1: The vertical grid-spacing, Δz as function of depth, z, for the three comparable resolutions, as well as for the new solar simulation with an z-scale optimized to capture the temperature structure.

In Fig. 1 I have also over-plotted the $P_{\rm turb}/P_{\rm tot}$-ratios (on an arbitrary scale) to illustrate the region which needs the best vertical sampling. Note how the sol100 pressure ratio lies about 100 km deeper than for the three others simulations - most likely a composition/opacity/mean-molecular-weight effect.

From Fig. 1 we see that comparisons between sol32, sol63 and sol125 are contaminated a little by distribution effects and the ruggedness of the sol125 z-

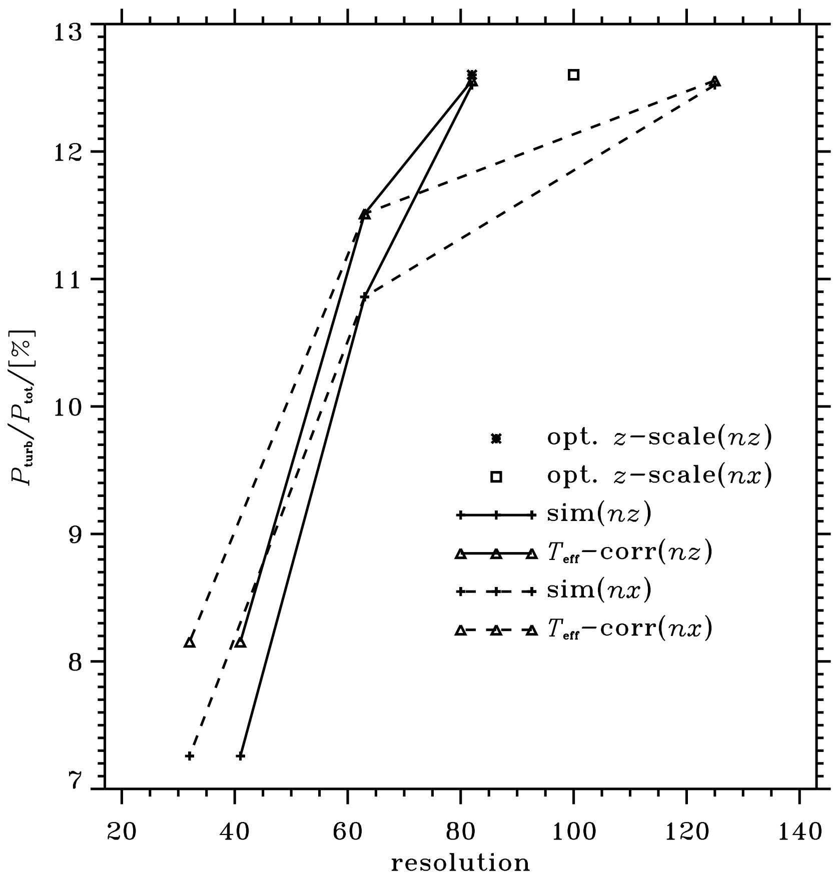

Figure 2: This plot shows the maximum of the $P_{\rm turb}/P_{\rm tot}$-ratio as function of the horizontal (dashed lines) and vertical (solid lines) resolutions, respectively. $+$'s indicate the raw data and $\triangle$'s have been corrected for the varying deviations from the solar $T_{\rm eff}$ and $g_{\rm surf}$. $*$ and $\square$ shows the position of the sol100 simulation in the diagram. The remaining differences between this latter and the three other simulations, is the chemical composition and the optimized z-scale.

scale. The sol100 z-scale has a much better sampling in the high gradient region and is furthermore differentiable, and gives a pressure ratio slightly larger than for sol125. The old and the optimized z-scales are compared in Sect. 3.

When studying Fig. 2, bear in mind that sol100 and sol125 have the same vertical resolution but differ in horizontal resolution which lower the turbulent pressure (*cf.* Sect. 4) and composition which slightly increases the turbulent pressure (*cf.* Sect. 5) of sol100 relative to sol125. The rest comes from the optimization of the z-grid, which is further analyzed in Sect. 3.

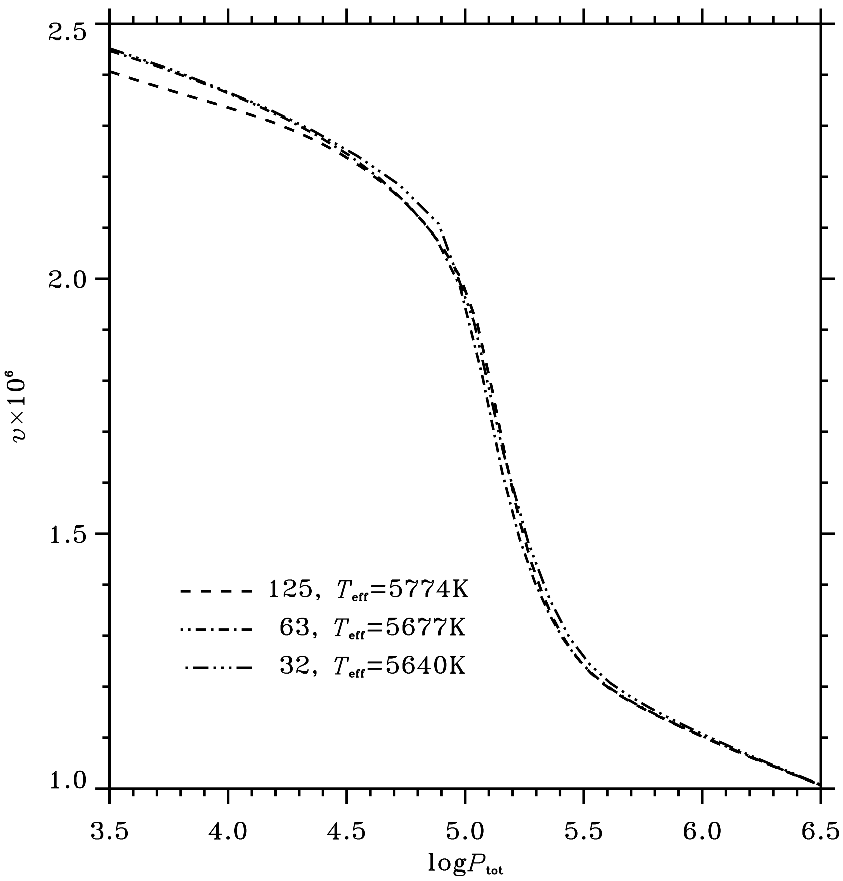

Figure 3: $\upsilon = \Gamma_1/c$, for the three comparable cases. Notice that the gradient in the photosphere steepens with resolution.

In Fig. 3 I have plotted $\upsilon = \Gamma_1/c$ for sol32, sol63 and sol125 to judge the effect on the oscillations. The lower υ high in the atmosphere of sol125 is probably due to bad statistics in the short 9:30 minutes averaging.

3 Effects of distribution of the z-points

The comparison in this section, is between Pro50z and Pro50 from Tab. 1, with Pro50z having a z-scale similar to sol32 and Pro50 having a z-scale similar to sol100 as depicted in Fig. 1.

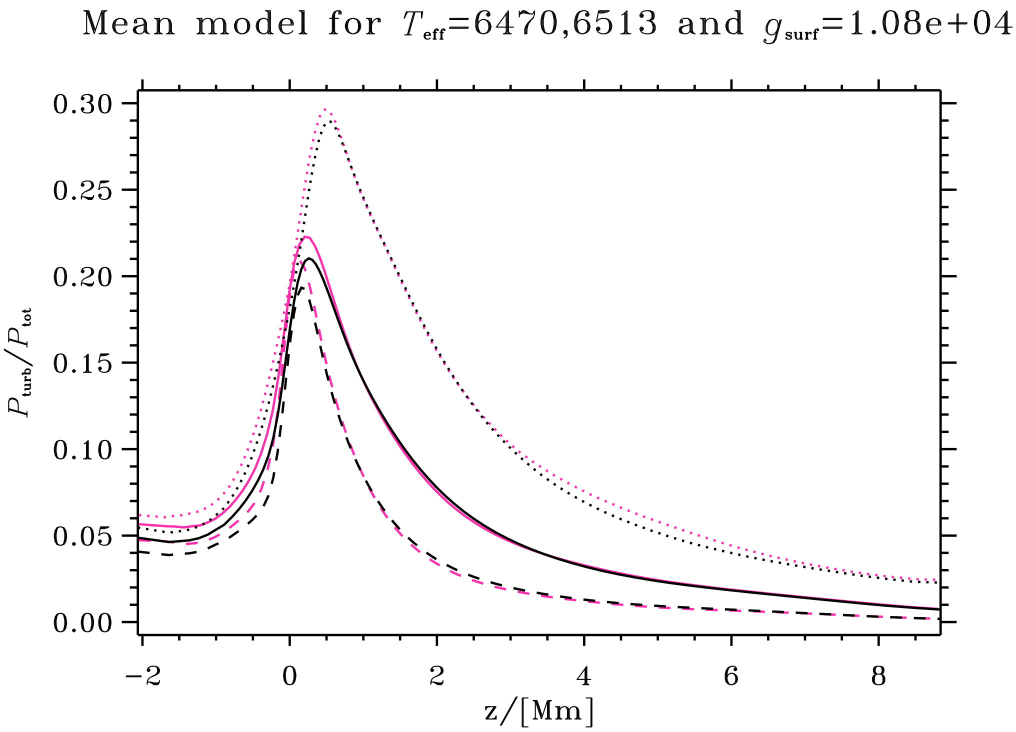

Figure 4: The turbulent- to total pressure ratio. Pink curves are for Pro50z and black curves for Pro50 with the optimized z-scale. I show both the total horizontal average (solid) as well as the average in the upflow (dashed) and the downflow (dotted).

From Fig. 4 we see that turbulent- to total pressure ratio actually decreases with better resolution in the photosphere — rather counterintuitive. If we correct for the differences in $T_{\rm eff}$ the difference decreases somewhat, to 1% (*cf.* Tab. 1). This decrease of $P_{\rm turb}$ can be explained by looking at the superadiabatic gradient in Fig. 5, which shows that $\nabla_{\rm s}$ increase with vertical resolution. The very sharp temperature gradient, in particular in the upflow, needs a very dense vertical grid, in order to get resolved, whereas the velocity field has less sharp features (*cf.* Figs. 6 and 7) and is therefore less demanding with respect to ver-

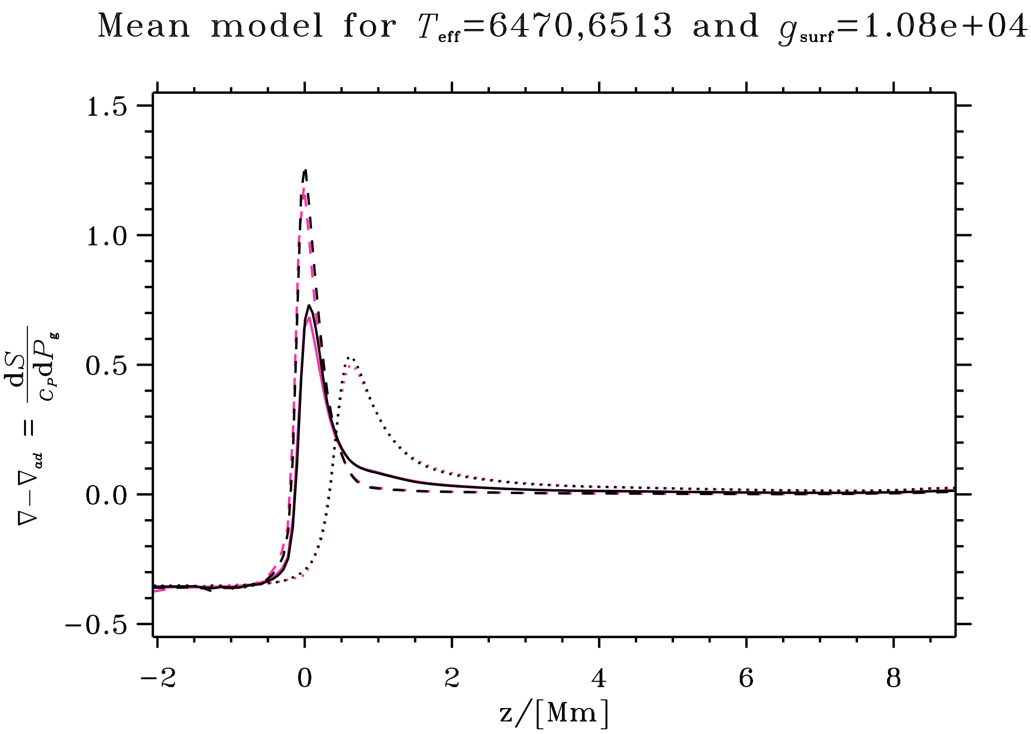

Figure 5: The superadiabatic gradient $\nabla_{\rm s}$. Pink curves are for Pro50z and black curves for Pro50 with the optimized z-scale. I show both the total horizontal average (solid) as well as the average in the upflow (dashed) and the downflow (dotted).

tical resolution. The introduction of the temperature optimized z-grid, is also accompanied by an optimized and differentiable grid for the radiative transfer, which might help in steepening the temperature gradient.

The larger $\nabla_{\rm s}$ means that the convective transport of energy gets more efficient, and therefore that the same flux can be achieved with lower velocities, which is clearly reflected in the vertical velocities in Fig. 6.

The horizontal velocities also decrease as the vertical velocities decrease because they just serve to maintain the density gradient by deflecting matter from the upflow sideways into the downflows (overturning).

The conclusion of this Section must be that the transport properties of the simulation changes with the distribution of vertical grid-points, because the sharp temperature gradient in the photosphere needs a good resolution. This is also reflected in the decrease in $T_{\rm eff}$ as the resolution in the photosphere increase.

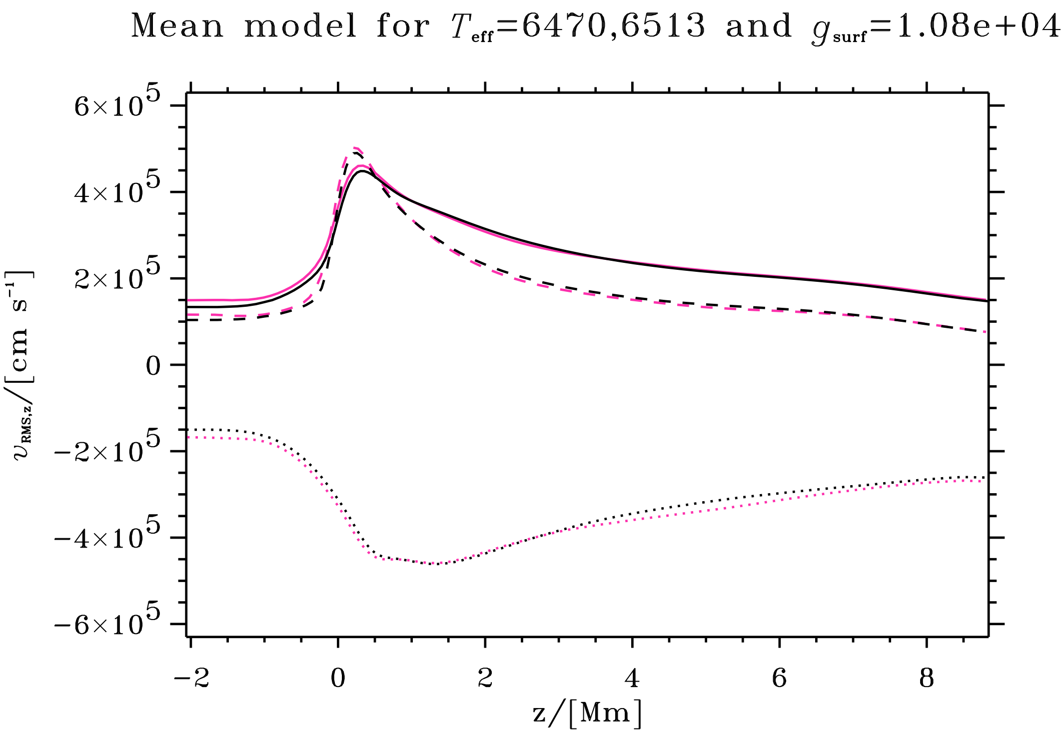

Figure 6: The vertical RMS velocity $v_{\mathrm{RMS},z}$. Pink curves are for Pro50z and black curves for Pro50 with the optimized z-scale. I show both the total horizontal average (solid) as well as the average in the upflow (dashed) and the downflow (dotted).

This decrease is too small though, to account for the decrease in velocities, which must still be ascribed to the increased efficiency of the convection, as discussed above.

We also see from Figs. 4-7 that the lower resolution in the deeper parts of Pro50 as compared to Pro50z, does not affect the structure significantly in this region, indicating that this redistribution of grid-points is closer to optimal.

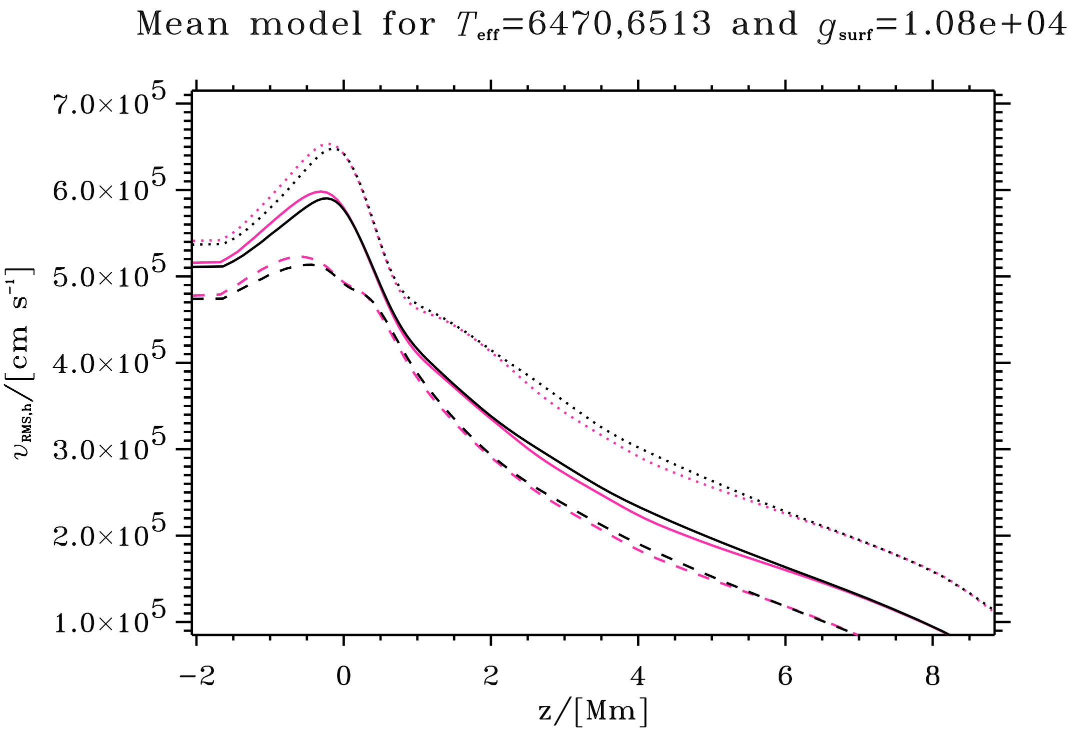

Figure 7: The horizontal RMS velocity $v_{\mathrm{RMS},h}$. Pink curves are for Pro50z and black curves for Pro50 with the optimized z-scale. I show both the total horizontal average (solid) as well as the average in the upflow (dashed) and the downflow (dotted).

4 Horizontal resolution

In this section I present the effect of doubling the horizontal resolution, going from sol50 to sol100.

From Fig. 8 we see that the turbulent pressure increase appreciable with increasing horizontal resolution, and the increase amounts to 1.6% when correcting for the 20 K difference in $T_{\rm eff}$. We also notice that most of this increase occurs in the downflows, which because of their intermittency and turbulent structures are much more sensitive to the horizontal resolution than are the fairly wellordered upflows. The upflow is probably mainly affected by conservation constraints.

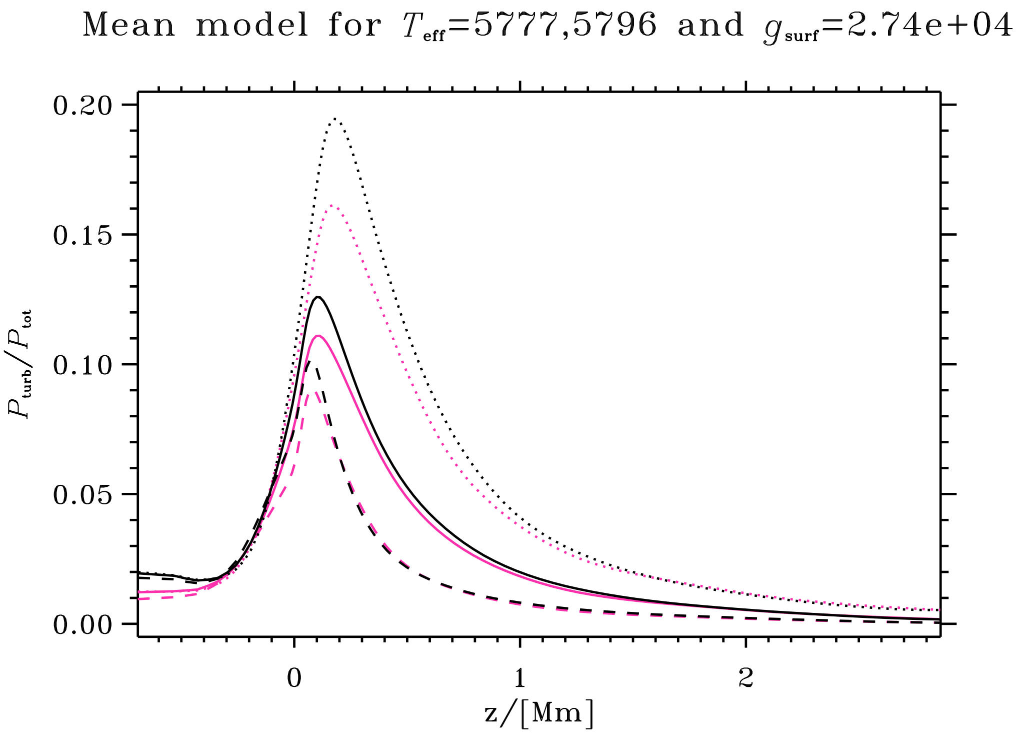

Figure 8: The turbulent- to total pressure ratio. Pink curves are for sol50 and black curves for sol100. I show both the total horizontal average (solid) as well as the average in the upflow (dashed) and the downflow (dotted).

The superadiabatic gradient displayed in Fig. 9 increases in the downflow and decrease in the upflow leading to a narrower range of gradients and a slight decrease in the overall gradient. As $\nabla_{\rm s}$ in the downflow peaks 126 km below the

∇_s-peak in the upflow, the former is likely to be smeared out in sol50 because of the small scale of the downflow structures. With higher resolution, higher temperature contrasts can be sustained, allowing for a larger gradient in the downflow. The broadening of the ∇_s-peak in the upflow, might be due to the

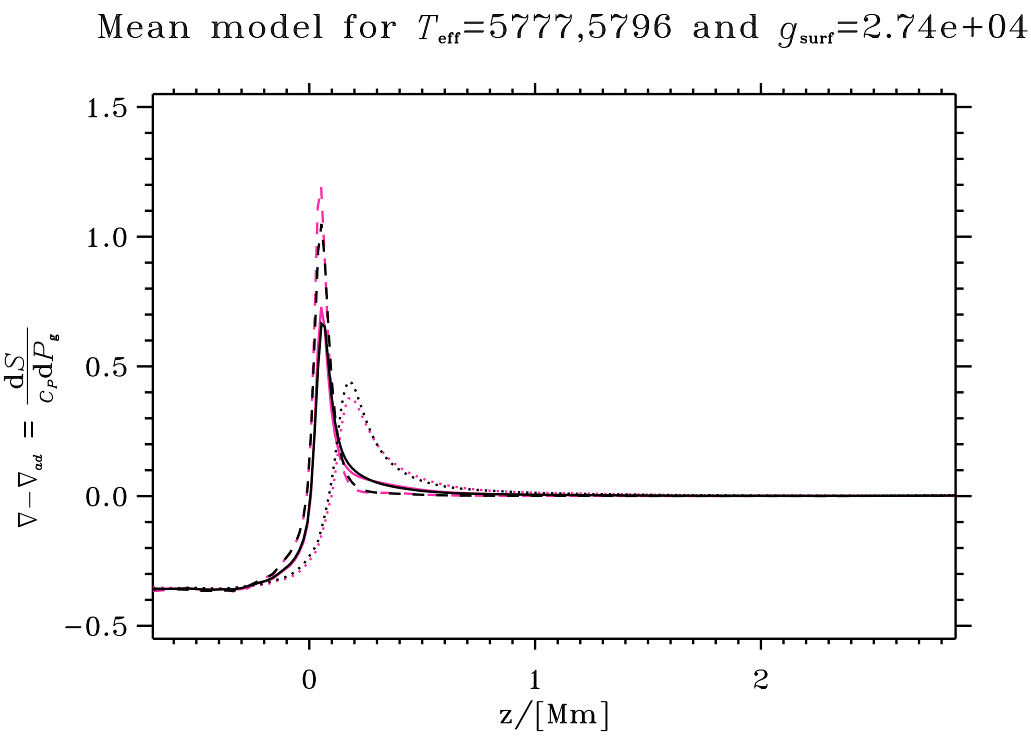

Figure 9: The superadiabatic gradient ∇_s. Pink curves are for sol50 and black curves for sol100. I show both the total horizontal average (solid) as well as the average in the upflow (dashed) and the downflow (dotted).

more efficient enthalpy transport in the downdrafts, prompting for more flux in the upflow. This increase of flux in the upflow is supplied both by an increase in the filling factor, *i.e.* the fractional area of matter taking part in the upflow, as well as an increase in ∇_s in the upflow at the height of the peak in the downflow ∇_s. The change in ∇_s in the upflow is somewhat counteracted by an small and almost symmetrical (*i.e.* opposite) change in the vertical velocities in the upflow (*cf.* Fig. 10).

The downflow speed is increased by about 8% from the top of the convection zone and down to a depth of about 2 Mm - more than twice as deep as the superadiabatic region. This increase in downdraft speed is probably necessary in order to maintain mass conservation, but also adds to the increase of flux in the downflow.

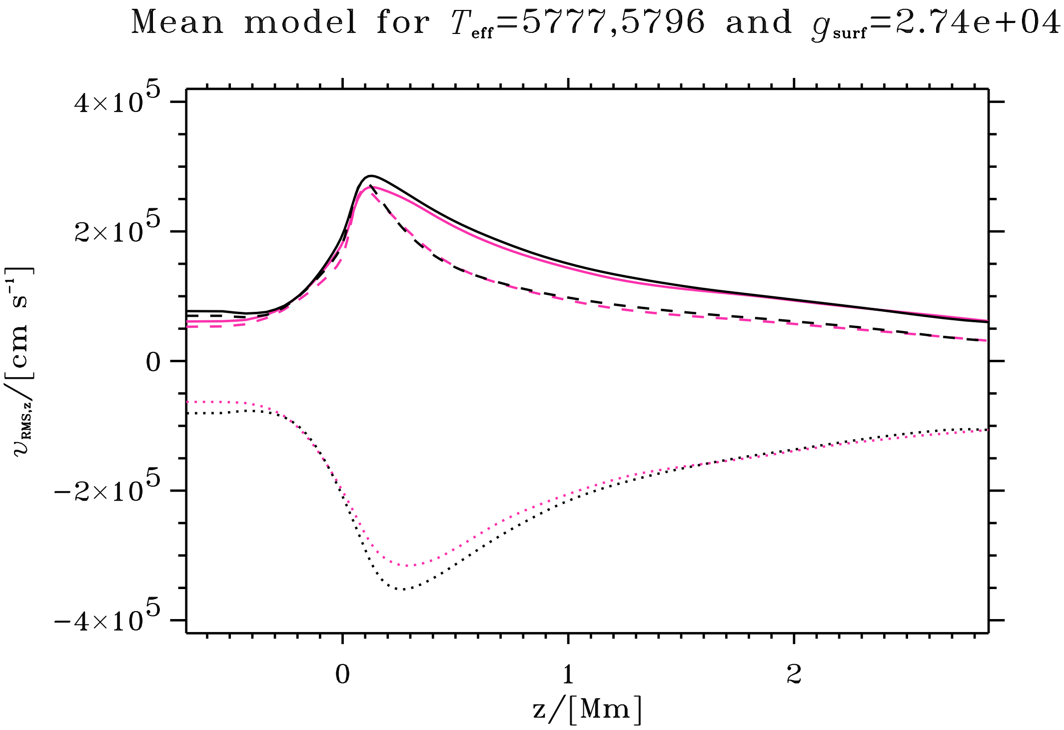

Figure 10: The vertical RMS velocity $v_{\mathrm{RMS},z}$. Pink curves are for sol50 and black curves for sol100. I show both the total horizontal average (solid) as well as the average in the upflow (dashed) and the downflow (dotted).

The horizontal velocities decrease though, which seems to violate mass conservation as the density stratification is hardly altered. The explanation lies in the fillingfactor. Near and just below the top of the convection zone, the fillingfactor is slightly larger for sun100, which means that a smaller amount of matter has to overturn to the downflow, hence the lower horizontal flow velocities.

The rearranging of fillingfactors and velocities, also cause the kinetic energy flux to increase, whereas the total enthalpy flux is basically unchanged, causing a net decrease in total flux, hence the 20 K decrease in $T_{\rm eff}$.

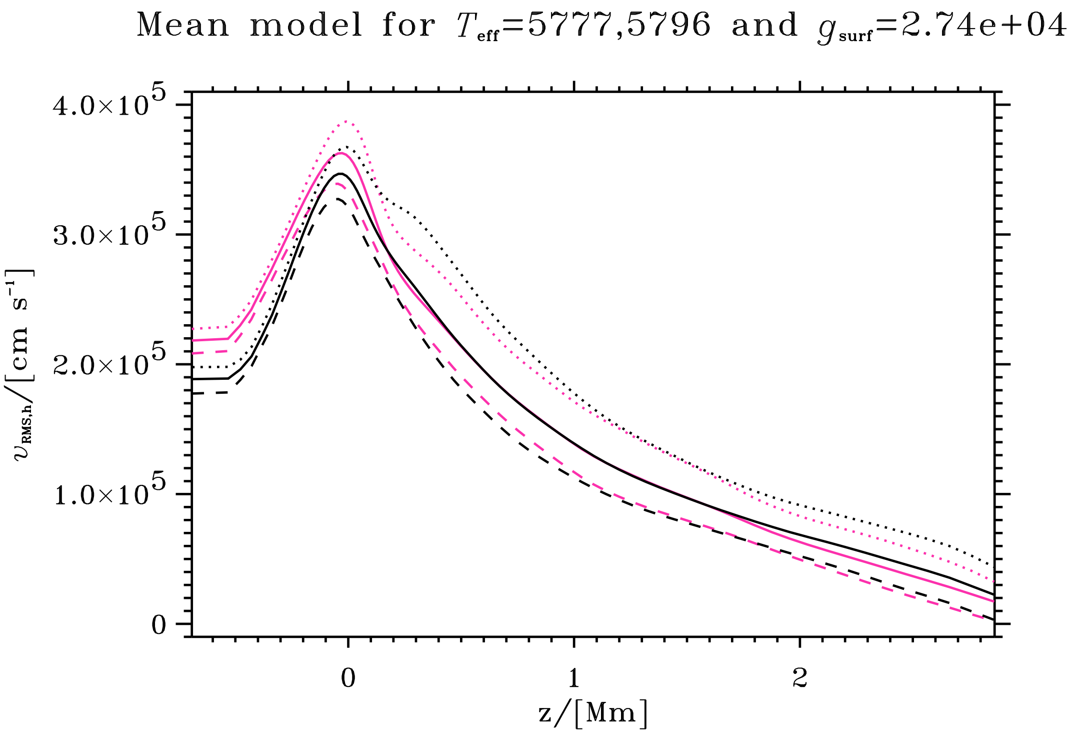

Figure 11: The horizontal RMS velocity $v_{\mathrm{RMS},h}$. Pink curves are for sol50 and black curves for sol100. I show both the total horizontal average (solid) as well as the average in the upflow (dashed) and the downflow (dotted).

5 Compositional effects

In this section I compare the effects of changing composition from the old Gustafsson mixture ($X = 70.2959\%$, $Y = 27.9161\%$), to the AG89 mixture and $Z/X = 0.0245$ and $Y = 24.5\%$, by comparing the simulations sol50G and sol50.

There are two immediate effects of this change; The mean molecular weight, μ, decrease and the opacity increase because of the smaller content of the opacity-wise inert helium.

Hydrostatic equilibrium

$$\frac{\mathrm{d}P}{\mathrm{d}r} = -g\varrho, \tag{2}$$

results in an overall increase of the density by approximately the μ-ratio, as the

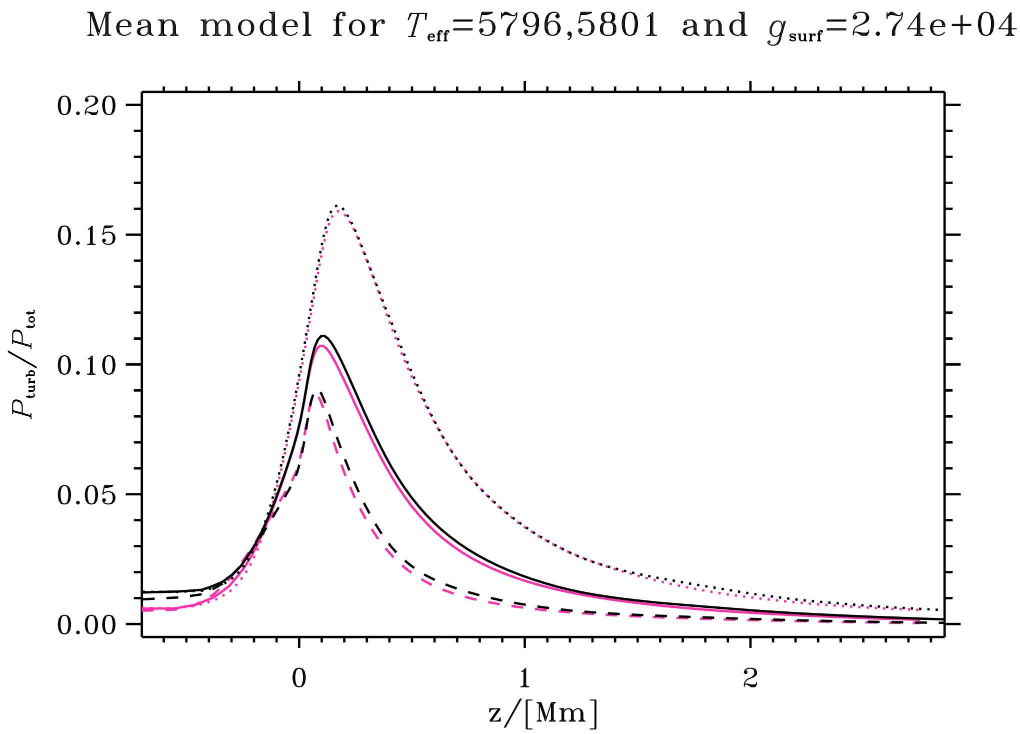

Figure 12: The turbulent- to total pressure ratio. Pink curves are for sol50 and black curves for sol50G. I show both the total horizontal average (solid) as well as the average in the upflow (dashed) and the downflow (dotted).

main part of the pressure

$$P = P_{\rm turb} + P_{\rm g} = \langle \varrho v_z^2 \rangle + \frac{\varrho k T}{\mu M_{\rm u}}, \tag{3}$$

is proportional to μ^{-1}. Dividing Eq. 2 with P we see that this causes a decrease in the pressure scale height

$$H_P = \frac{P}{g\varrho} = \frac{P_{\rm turb}}{g\varrho} + \frac{kT}{g\mu M_{\rm u}}, \tag{4}$$

which disappears with depth though, due to a rise in temperature. The first order effect is therefore a contraction of the atmosphere by the ratio of the μ's for the two cases. As the differences in composition also affects the ionization

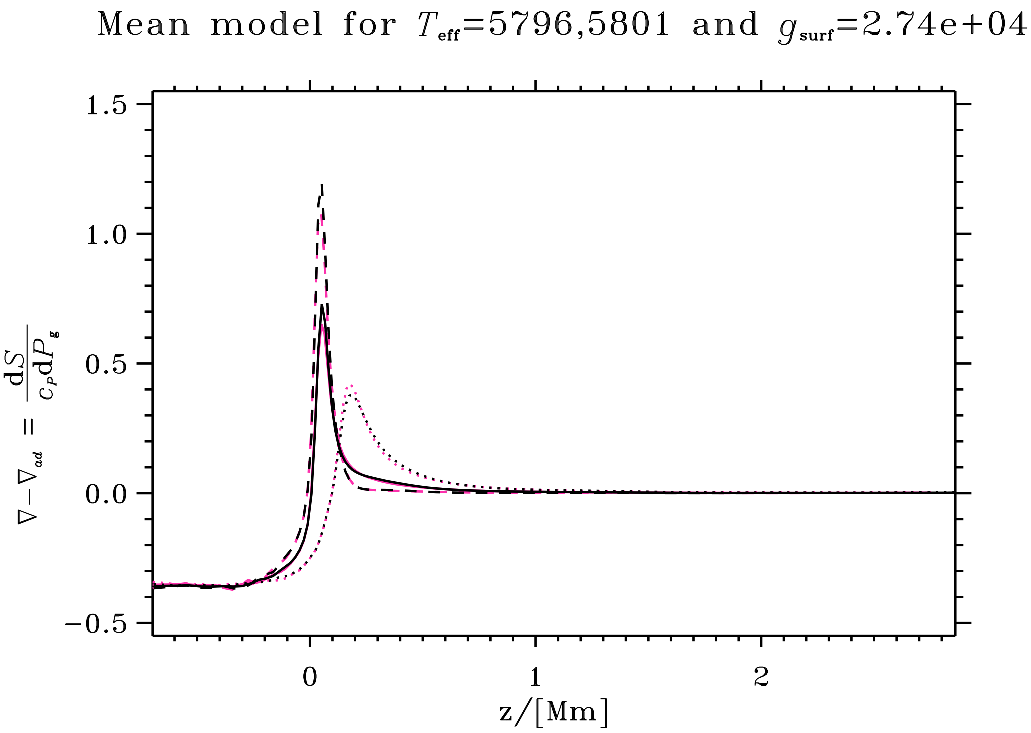

Figure 13: The superadiabatic gradient $\nabla_{\rm s}$. Pink curves are for sol50 and black curves for sol50G. I show both the total horizontal average (solid) as well as the average in the upflow (dashed) and the downflow (dotted).

structure, *i.e.* the μ ratio is not a constant but changes with depth, other effects enters too.

From Fig. 13 and 14 we see that both the super adiabatic gradient and the vertical velocities decrease, going from sol50G to sol50. The total flux is maintained at $T_{\rm eff} \simeq 5800$K though, because of the larger density. The $\nabla_{\rm s}$-peak in the downflow is increased whereas the peak in the upflow and the total average is decreased This is possible because the fillingfactor increases from the $\nabla_{\rm s}$-peak in the upflow and downwards, with about 3%, effectively broadening the peak in the total average of $\nabla_{\rm s}$.

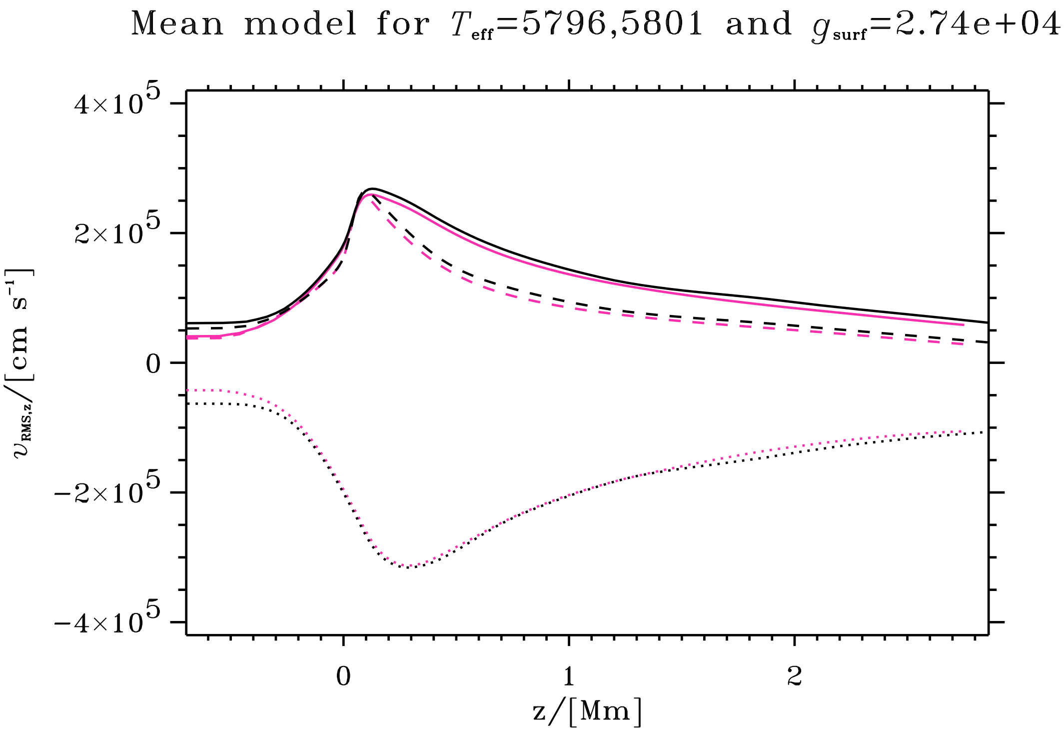

Figure 14: The vertical RMS velocity $v_{{\rm RMS},z}$. Pink curves are for sol50 and black curves for sol50G. I show both the total horizontal average (solid) as well as the average in the upflow (dashed) and the downflow (dotted).

The horizontal velocities are in general smaller, but not by the same constant factor as is the case for the vertical velocities in the upflow, because of the changing fillingfactor.

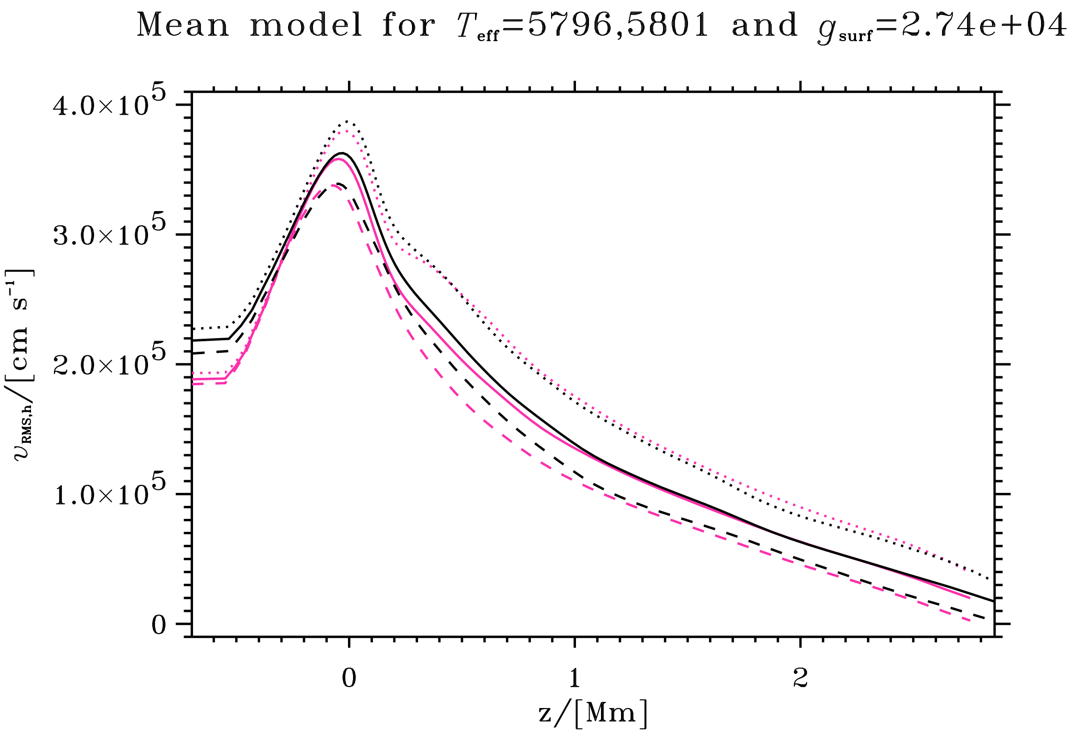

Figure 15: The horizontal RMS velocity $v_{\mathrm{RMS},h}$. Pink curves are for sol50 and black curves for sol50G. I show both the total horizontal average (solid) as well as the average in the upflow (dashed) and the downflow (dotted).